IOPscience iopscience.iop.org

Home Search Collections Journals About Contact us My IOPscience

The asymptotic transfer method in the envelope function approximation

This article has been downloaded from IOPscience. Please scroll down to see the full text article.

1989 J. Phys.: Condens. Matter 1 7335

(http://iopscience.iop.org/0953-8984/1/40/009)

View the table of contents for this issue, or go to the journal homepage for more

Download details:
IP Address: 171.66.16.96
The article was downloaded on 10/05/2010 at 20:23

Please note that terms and conditions apply.

J. Phys.: Condens. Matter 1 (1989) 7335–7345. Printed in the UK

The asymptotic transfer method in the envelope function approximation

Guoyi Qin
Center of Theoretical Physics, The Laboratory of Solid State Microstructure, Nanjing University, Nanjing, People's Republic of China

Received 3 January 1989

Abstract. It is pointed out that, in terms of the successive product of a great number of transfer matrices, the electron subbands and wavefunctions can be solved consistently for type-I or type-II semiconductor systems in which the band edges of conduction bands and valence bands are not flat (oblique lines or curves). As an illustrative example, we performed a self-consistent calculation of electron subbands and wavefunctions of the $Ga_{1-x}Al_xAs$ sawtooth superlattice taking account of the variation in the effective mass of electrons with the concentration of Al.

1. Introduction

In [1], we derived the transfer matrix suitable for both type-I and type-II semiconductor multi-layer systems that connect the amplitudes of the wavefunction of the lth layer to that of the $(l+1)$th layer. In terms of the successive product of a series of transfer matrices, the electron subbands and wavefunctions of multi-layer systems, such as superlattices or quasi-periodic superlattices, can be determined.

We suggested that this type of method could be generalised to deal with semiconductor systems in which the edges of conduction bands and valence bands are not flat (oblique lines or curves). For example, if an electric field is applied along the growth axis of a multi-quantum-well system [2], the edges of the conduction bands and valence bands of each quantum well decline. We cannot obtain solutions of the two-band envelope function equation (equation (1) in § 2), even for a single well or barrier, nor can all these solutions of wells and barriers be connected to obtain the secular equation of the whole system by means of boundary conditions.

However, if we divide the width of each well and barrier into a large number of sublayers, because the width of each sublayer is very small we can consider approximately that the energy values of the edges of the conduction bands and valence bands are constant within each sublayer but differ from those of their nearest neighbours. So the band edges of the whole system could be expressed approximately by a series of flights of stairs, each flight of stairs containing a number of flat steps. The envelopes of these flights of stairs are simply the real shapes of the band edges. Now it is easy to see that, after this type of division, systems in which the band edges are not flat are equivalent approximately to multi-sublayer systems. Therefore, in terms of the method presented

0953-8984/89/407335 + 11 $02.50 © 1989 IOP Publishing Ltd

in [1] the electron subbands and wavefunctions of these systems can be determined. We call this type of method the asymptotic transfer method (ATM).

2. Theory

For type-II semiconductor periodic systems with period D in which the band edges have complex shapes. Electron subbands and wavefunctions can be determined from the two-band envelope function equation [1]:

$$\begin{bmatrix} H_{11}(\varepsilon) & H_{12}(\varepsilon) \\ H_{21}(\varepsilon) & H_{22}(\varepsilon) \end{bmatrix} \begin{bmatrix} F_1(\varepsilon) \\ F_2(\varepsilon) \end{bmatrix} = \varepsilon \begin{bmatrix} F_1(\varepsilon) \\ F_2(\varepsilon) \end{bmatrix} \tag{1}$$

where

$$\begin{aligned} H_{11}(\varepsilon) = H_{22}(\varepsilon) &= V_s(z) + \Pi^2 K_-[\varepsilon_g + \varepsilon - V_p(z)]^{-1} K_+ \\ &\quad + \tfrac{1}{3}\Pi^2 K_+[\varepsilon_g + \varepsilon - V_p(z)]^{-1} K_- + \tfrac{2}{3}\Pi^2 K_z[\varepsilon_g + \varepsilon - V_p(z)]^{-1} K_z \end{aligned} \tag{2}$$

$$\begin{aligned} H_{12}^*(\varepsilon) = H_{21}(\varepsilon) &= (\sqrt{2}/3)\Pi^2\{K_z[\varepsilon_g + \varepsilon - V_p(z)]^{-1} K_+ \\ &\quad - K_+[\varepsilon_g + \varepsilon - V_p(z)]^{-1} K_z\} \end{aligned} \tag{3}$$

$$K_\pm = (1/\sqrt{2})(K_x \pm \mathrm{i}\, K_y) \qquad K_z = -\mathrm{i}\,\mathrm{d}/\mathrm{d}z. \tag{4}$$

The Kane matrix element

$$\Pi = (\hbar/m_0)\langle \mathrm{i}S|\hat{p}_z|z\rangle. \tag{5}$$

ε_g is the energy gap of this system, $V_s(z)$ and $V_p(z)$ are the energy values of the band edges of conduction band and valence band, respectively, as functions of z, and the z axis is chosen to lie along the growth axis of the system.

Now, we divide the width D of the primary cell into j sublayers for instance. If j is large enough, the width of each sublayer is very small. Within each sublayer, the lth sublayer for instance, the energies $V_s^l(z)$ and $V_p^l(z)$ of the edges of conduction band and valence band can be considered as constant: V_s^l and V_p^l. So $H_{12}(\varepsilon) = 0$ and $H_{21}(\varepsilon) = 0$, and equation (1) can be reduced to two separate equations

$$(\mathrm{d}^2/\mathrm{d}z^2 + \alpha_l^2)F_1^l(z) = 0 \tag{6a}$$

$$(\mathrm{d}^2/\mathrm{d}z^2 + \alpha_l^2)F_2^l(z) = 0 \tag{6b}$$

where

$$\alpha_l^2 = -(3/2\Pi^2)(\varepsilon_g + \varepsilon - V_p^l)(V_s^l - \varepsilon) - \boldsymbol{K}_\perp^2 \tag{7}$$

in which $\boldsymbol{K}_\perp$ is the wavevector in the plane perpendicular to the z axis. The solutions of equation (6) in the lth sublayer are

$$\begin{aligned} F_1^l(\boldsymbol{r}, z) &= \{A_1^l \exp[\mathrm{i}\,\alpha_l(z - z_l)] + B_1^l \exp[-\mathrm{i}\,\alpha_l(z - z_l)]\} \exp(\mathrm{i}\boldsymbol{K}_\perp \cdot \boldsymbol{r}) \\ F_2^l(\boldsymbol{r}, z) &= \{A_2^l \exp[\mathrm{i}\alpha_l(z - z_l)] + B_2^l \exp[-\mathrm{i}\,\alpha_l(z - z_l)]\} \exp(\mathrm{i}\boldsymbol{K}_\perp \cdot \boldsymbol{r}) \end{aligned} \tag{8}$$

where $\boldsymbol{r}$ is the two-dimensional coordinate vector in the $x-y$ plane.

In terms of the four continuity conditions of wavefunctions in the interface, the amplitudes of the wavefunctions of the lth sublayer can be connected to those of the $(l+1)$th sublayer via a transfer matrix $\mathbf{T}_l$

$$\begin{bmatrix} \tilde{A}_1^{l+1} \\ \tilde{B}_1^{l+1} \\ \tilde{B}_2^{l+1} \\ \tilde{A}_2^{l+1} \end{bmatrix} = \mathbf{T}_l \begin{bmatrix} \tilde{A}_1^{l} \\ \tilde{B}_1^{l} \\ \tilde{B}_2^{l} \\ \tilde{A}_2^{l} \end{bmatrix} \tag{9}$$

where $\tilde{A}_1^l$, etc, are the reduced amplitudes of wavefunctions defined as

$$\tilde{A}_1^l = (\alpha_l/M^l)^{1/2} A_1^l \qquad \tilde{B}_1^l = (\alpha_l/M^l)^{1/2} B_1^l \qquad \text{etc}$$

and

$$\tilde{A}_1^{l+1} = (\alpha_{l+1}/M^{l+1})^{1/2} A_1^{l+1} \qquad \tilde{B}_1^{l+1} = (\alpha_{l+1}/M^{l+1})^{1/2} B_1^{l+1} \qquad \text{etc}$$

in which

$$M^l = (\varepsilon_g + \varepsilon - V_p^l) \tag{10}$$

and the transfer matrix is

$$\mathbf{T}_l = \begin{bmatrix} J_l \exp(\mathrm{i}\alpha_l d_l) & \theta_l \exp(-\mathrm{i}\alpha_l d_l) & -R_l \exp(-\mathrm{i}\alpha_l d_l) & -R_l \exp(\mathrm{i}\alpha_l d_l) \\ \theta_l \exp(\mathrm{i}\alpha_l d_l) & J_l \exp(-\mathrm{i}\alpha_l d_l) & R_l \exp(-\mathrm{i}\alpha_l d_l) & \exp(\mathrm{i}\alpha_l d_l) \\ -R_l^- \exp(\mathrm{i}\alpha_l d_l) & -R_l^- \exp(-\mathrm{i}\alpha_l d_l) & J_l \exp(-\mathrm{i}\alpha_l d_l) & \theta_l \exp(\mathrm{i}\alpha_l d_l) \\ R_l^- \exp(\mathrm{i}\alpha_l d_l) & R_l^- \exp(-\mathrm{i}\alpha_l d_l) & \theta_l \exp(-\mathrm{i}\alpha_l d_l) & J_l \exp(\mathrm{i}\alpha_l d_l) \end{bmatrix} \tag{11}$$

where

$$\begin{aligned} J_l &= \tfrac{1}{2}[(\alpha^{\mathrm{R}}/M^{\mathrm{R}})^{1/2} + (M^{\mathrm{R}}/\alpha^{\mathrm{R}})^{1/2}] \\ \theta_l &= \tfrac{1}{2}[(\alpha^{\mathrm{R}}/M^{\mathrm{R}})^{1/2} - (M^{\mathrm{R}}/\alpha^{\mathrm{R}})^{1/2}] \end{aligned} \tag{12}$$

$$\begin{aligned} R_l &= \tfrac{1}{2}[K_+/(2\alpha_l\alpha_{l+1})^{1/2}][(1/M^{\mathrm{R}})^{1/2} - (M^{\mathrm{R}})^{1/2}] \\ R_l^- &= \tfrac{1}{2}[K_-/(2\alpha_l\alpha_{l+1})^{1/2}][(1/M^{\mathrm{R}})^{1/2} - (M^{\mathrm{R}})^{1/2}] \end{aligned} \tag{13}$$

and

$$\alpha^{\mathrm{R}} = \alpha_{l+1}/\alpha_l \qquad M^{\mathrm{R}} = M^{l+1}/M^l. \tag{14}$$

In equation (11), d_l is the width of the lth sublayer.

By means of the successive product of j transfer matrices and after introducing the Bloch index $\mathcal{K}$, we obtain a secular-like equation

$$\begin{bmatrix} (\mathbf{M}_j)_{11} - \mathrm{e}^{\mathrm{i}\mathcal{K}D} & (\mathbf{M}_j)_{12} & (\mathbf{M}_j)_{13} & (\mathbf{M}_j)_{14} \\ (\mathbf{M}_j)_{21} & (\mathbf{M}_j)_{22} - \mathrm{e}^{\mathrm{i}\mathcal{K}D} & (\mathbf{M}_j)_{23} & (\mathbf{M}_j)_{24} \\ (\mathbf{M}_j)_{31} & (\mathbf{M}_j)_{32} & (\mathbf{M}_j)_{33} - \mathrm{e}^{\mathrm{i}\mathcal{K}D} & (\mathbf{M}_j)_{34} \\ (\mathbf{M}_j)_{41} & (\mathbf{M}_j)_{42} & (\mathbf{M}_j)_{43} & (\mathbf{M}_j)_{44} - \mathrm{e}^{\mathrm{i}\mathcal{K}D} \end{bmatrix} \begin{bmatrix} \tilde{A}_1^1 \\ \tilde{B}_1^1 \\ \tilde{B}_2^1 \\ \tilde{A}_2^1 \end{bmatrix} = 0 \tag{15}$$

where

$$\mathbf{M}_j = \prod_{l=1}^{j} \mathbf{T}_l. \tag{16}$$

For type-I systems, such as GaAs–$Ga_{1-x}Al_xAs$, the interaction between the conduction and valence bands is small because of the large energy gap ($\varepsilon_g = 1.5$ eV); as a result the motion perpendicular to the interfaces of sublayers is hardly affected by the motion parallel to the interface. Hence we need only consider the case when $K_\perp = 0$. In this case, R_l and R_l^- of equation (11) are equal to zero. $\mathbf{T}_l$ in equation (11) reduces to two disconnected 2×2 submatrices, one of which is

$$\mathbf{T}_l = \begin{bmatrix} J_l \exp(\mathrm{i}\alpha_l d_l) & \theta_l \exp(-\mathrm{i}\alpha_l d_l) \\ \theta_l \exp(\mathrm{i}\alpha_l d_l) & J_l \exp(-\mathrm{i}\alpha_l d_l) \end{bmatrix} \tag{17}$$

and the secular-like equation becomes

$$\begin{pmatrix} (\mathbf{M}_j)_{11} - \exp(\mathrm{i}\mathcal{K}D) & (\mathbf{M}_j)_{12} \\ (\mathbf{M}_j)_{21} & (\mathbf{M}_j)_{22} - \exp(\mathrm{i}\mathcal{K}D) \end{pmatrix} \begin{pmatrix} \tilde{A}_1^1 \\ \tilde{B}_1^1 \end{pmatrix} = 0. \tag{18}$$

Further, if

$$(2\Pi^2/3)(\varepsilon_g + \varepsilon - V_p^l)^{-1} \simeq 1/2m_l^{e*} \tag{19}$$

equation (6*a*) becomes

$$(\mathrm{d}^2/\mathrm{d}z^2 + \beta_l^2)F_1^l(z) = 0 \tag{20}$$

where

$$\beta_l^2 = (2m_l^{e*}/\hbar^2)(\varepsilon - V_s^l) \tag{21}$$

in which m_l^{e*} is the effective mass of electrons in the lth sublayer.

The transfer matrix in equation (17) reduces to

$$\mathbf{T}_l^{(e)} = \begin{bmatrix} I_l \exp(\mathrm{i}\beta_l d_l) & I_l^- \exp(-\mathrm{i}\beta_l d_l) \\ I_l^- \exp(\mathrm{i}\beta_l d_l) & I_l \exp(-\mathrm{i}\beta_l d_l) \end{bmatrix} \tag{22}$$

where

$$I_l = \tfrac{1}{2}(f_l^{1/2} + f_l^{-1/2}) \qquad I_l^- = (f_l^{1/2} - f_l^{-1/2}) \tag{23}$$

and

$$f_l = (m_{l+1}^{e*}/m_l^{e*})/(\beta_{l+1}/\beta_l). \tag{24}$$

The secular-like equation becomes

$$\begin{pmatrix} (\mathbf{M}_j^{(e)})_{11} - \exp(\mathrm{i}\mathcal{K}D) & (\mathbf{M}_j^{(e)})_{12} \\ (\mathbf{M}_j^{(e)})_{21} & (\mathbf{M}_j^{(e)})_{22} - \exp(\mathrm{i}\mathcal{K}D) \end{pmatrix} \begin{pmatrix} \tilde{A}_1^1 \\ \tilde{B}_1^1 \end{pmatrix} = 0 \tag{25}$$

where

$$\mathbf{M}_j^{(e)} = \prod_{l=1}^{j} \mathbf{T}_l^{(e)}. \tag{26}$$

Hence, we can see that taking account of the variation in both the conduction band and valence band energies $V_s(z)$ and $V_p(z)$ as functions of z at the same time is equivalent

approximately to considering the variation in the effective mass of electrons as a function of z in each primary cell.

To solve the problem self-consistently, we must also know the subbands and wavefunctions of holes in the valence band. Following [3], when $\boldsymbol{K}_\perp = 0$, the parabolic single-band envelope function equation for holes is

$$[\mathrm{d}^2/\mathrm{d}Z^2 + \tilde{\beta}_l(Z)]F_1^l(Z) = 0 \tag{27}$$

where

$$\tilde{\beta}_l^2(z) = 2m_l^{\mathrm{h}*}/\hbar^2(\varepsilon - V_\mathrm{p}^l) \tag{28}$$

in which $m_l^{\mathrm{h}*}$ is the effective mass of holes in the lth sublayer. Then the corresponding transfer matrix for wavefunctions of holes is

$$\mathbf{T}_l^{(\mathrm{h})} = \begin{bmatrix} \tilde{I}_l \exp(\mathrm{i}\tilde{\beta}_l d_l) & \tilde{I}_l^- \exp(-\mathrm{i}\tilde{\beta}_l d_l) \\ \tilde{I}_l^- \exp(\mathrm{i}\tilde{\beta}_l d_l) & \tilde{I}_l \exp(-\mathrm{i}\tilde{\beta}_l d_l) \end{bmatrix} \tag{29}$$

where

$$\tilde{I}_l = \tfrac{1}{2}(\tilde{f}_l^{1/2} + \tilde{f}_l^{-1/2}) \qquad \tilde{I}_l^- = \tfrac{1}{2}(\tilde{f}_l^{1/2} - \tilde{f}_l^{-1/2}) \tag{30}$$

and

$$\tilde{f}_l = (m_{l+1}^{\mathrm{h}*}/M_l^{\mathrm{h}*})/(\tilde{\beta}_{l+1}/\beta_l). \tag{32}$$

The secular-like equation becomes

$$\begin{pmatrix} (\mathbf{M}_j^{(\mathrm{h})})_{11} - \exp(\mathrm{i}\mathcal{K}D) & (\mathbf{M}_j^{(\mathrm{h})})_{12} \\ (\mathbf{M}_j^{(\mathrm{h})})_{21} & (\mathbf{M}_j^{(\mathrm{h})})_{22} - \exp(\mathrm{i}\mathcal{K}D) \end{pmatrix} \begin{pmatrix} \tilde{A}_1^1 \\ \tilde{B}_1^1 \end{pmatrix} = 0 \tag{32}$$

where

$$\mathbf{M}_j^{(\mathrm{h})} = \prod_{l=1}^{j} \mathbf{T}_l^{(h)}. \tag{33}$$

The ATM is suitable for non-period systems too. In this case we can divide the whole system into j sublayers and then solve the coupled equations of equation (15) and two boundary conditions at both terminations of the system to determine the subbands and wavefunctions of electrons.

As an illustrative example, in this paper we perform a self-consistent calculation of electron subbands for the type-I $\mathrm{GaAs}_{1-x}\mathrm{Al}_x\mathrm{As}$ sawtooth superlattice.

3. Electron subbands of sawtooth superlattice

In [4] is presented a quantum mechanics theory to calculate the electron subbands of GaAs–$\mathrm{Ga}_{1-x}\mathrm{Al}_x\mathrm{As}$ sawtooth superlattice in which the Al concentration x is proportional to the coordinate z within each period D, resulting in a sawtooth shape of both the conduction band and the valence band. At the end of each D the energies of the

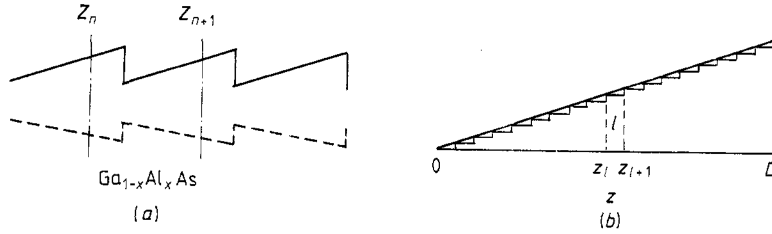

Figure 1. (*a*) The sketch of the structure of the band edges of the GaAs–$Ga_{1-x}Al_xAs$ sawtooth superlattice. (*b*) In ATM, the real band edge of a primary cell of sawtooth superlattice is replaced by a flight of stairs containing j flat plateaus. The larger j, the more accurate are the results of ATM. In this figure we take $j = 18$ as an illustrative example.

conduction band and valence band have the extreme values shown in figure 1(*a*). The same problem will again be discussed here as an illustrative example of ATM. In comparison with the results in [4] the ATM results have improved in three ways.

(i) The variations in both the conduction band edge and the valence band edge are taken into account. As we have discussed above, this is equivalent approximately to taking account of the variation in effective mass of electrons as function of z in each period.

(ii) ATM can determine the electron subbands self-consistently but the method of ordinary quantum mechanics cannot.

(iii) The variation in effective mass of holes with the concentration of Al in each period can be considered by ATM, but it cannot be considered by the method in [4].

The primary cell of this system has width D. We divide each primary cell of the sawtooth superlattice into j sublayers, as shown in figure 1(*b*). Because j is a larger number, within any sublayer (the lth sublayer for instance), $V_s(z)$ and $V_p(z)$ can be considered approximately as constant, i.e. $V_s^l(z) = V_s^l$ and $V_p^l(z) = V_p^l$.

According to the formula given in [5]

$$\varepsilon_g(x) = 1519.2 + 1247x \quad \text{(meV)} \tag{34}$$

where x is the concentration of Al in $Ga_{1-x}Al_xAs$. And the band offsets used are 60% and 40% of the band-gap difference between the conduction and valence bands, respectively. If we take $x = 0.2$, the extreme energy values of the conduction band and valence band in each primary cell are

$$\begin{aligned} V_s^{\max} &= 249.4 \times 60\% = 149.64 \quad \text{(meV)} \\ V_p^{\min} &= -249.4 \times 40\% = -99.76 \quad \text{(meV)}. \end{aligned} \tag{35}$$

To compare our results with those in [4] to check the accuracy of ATM, we put $m_l^{e^*}$ equal to a constant first:

$$m_l^{e^*} = 0.067 m_0 \tag{36}$$

where m_0 is the mass of free electrons.

The band edge of the conduction band in the lth sublayer is

$$V_s^l(z) = V_s^l = 149.64[(l-1)/j]. \tag{37}$$

If we put equations (36) and (37) into the single-band envelope function equation

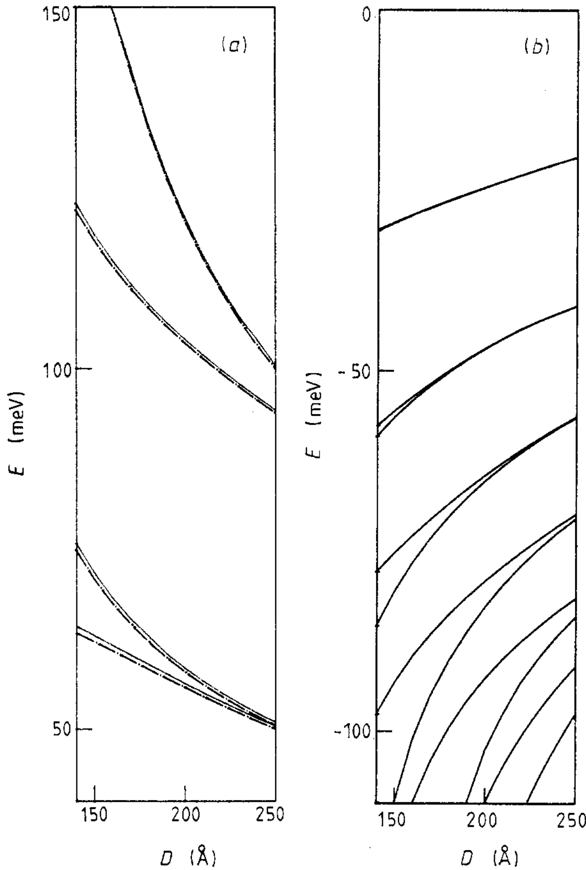

Figure 2. (*a*) A plot of subband energies and band widths for electrons as a function of the period in a sawtooth superlattice calculated by ATM (the parameters are $m^{e^*} = 0.067\, m_0$, $x = 0.2$, $j = 100$, $j = 200$ for broken curves and for full curves). (*b*) A plot of subband energies and bandwidth for heavy holes as a function of the period in sawtooth superlattice calculated by ATM. The parameters are $m^{h^*} = 0.45 m_0$, $x = 0.2$ and $j = 200$.

for electrons (equations (20) and (21)), then using equations (22)–(26) the subbands and wavefunctions of electrons in the sawtooth superlattice can be determined. The results for electron subbands are shown in figure 2(*a*). The broken curves are obtained from the calculation in which the number of sublayers in each primary cell is $j = 100$, and the full curves are obtained from the calculation in which $j = 200$. The full curves nearly reproduce the results of the analytic method in [4]. The energy difference between results (the full curves in figure 2(*a*)) and those in [4] is less than 0.3 meV for the ground sub-band in the region from $D = 140$ Å to $D = 250$ Å.

In the same way, if we take the effective mass of heavy holes as constant, i.e.

$$m_l^{h^*} = 0.45 m_0 \tag{38}$$

the band edge of the valence band is given by

$$V_p^l(z) = V_p^l = -99.76[(l-1)/j]. \tag{39}$$

If we put equations (38) and (39) into equations (28)–(33), the subbands and wavefunctions of heavy holes can be determined. The results are shown in figure 2(*b*). The parameters taken now are $j = 200$. The results plotted in figure 2(*b*) also approximately reproduce the results in [4], especially for the ground subband of heavy holes. All the results given above prove that ATM is a good approximation of the rigorous

analytical method when the gradients of the band edges as function of z are not too large. The accuracy depends on the parameter

$$\lambda = L/w \tag{40}$$

where L is the energy leap between neighbouring sublayers and w is the width of each sublayer. The smaller λ, the more accurate are the results of ATM. In our calculation, we chose the number j to give $\lambda = 1$ meV Å^{-1}. It seems that this is sufficient for our purpose.

Then, we take the variation in both the conduction band and the valence band into account. As we have discussed in § 2, for type-I semiconductor systems, this is equivalent approximately to taking account of the variation in the effective mass of electrons. According to equation (35), in the lth sublayer

$$\begin{aligned} V_s^l &= 149.64[(l-1)/j] \\ V_p^l &= -99.76[(l-1)/j] \end{aligned} \tag{41}$$

and we take the Kane matrix element of GaAs to be

$$\Pi = (\hbar/m_0)\langle iS|\hat{p}_z|z\rangle = 1.076 \times 10^{-4} \quad (\text{meV cm}). \tag{42}$$

By substitution of equations (41) and (42) into equations (16) and (18), the subbands and wavefunctions of electrons taking account of the variation in effective mass are obtained.

For heavy holes, if we take account of its effective mass as a function of z. According to the formula given in [3]

$$m^{h^*}(x) = [m^{h^*}(\text{GaAs}) + 0.31x]m_0. \tag{43}$$

When we take $x = 0.2$ amd $m^{h^*}(\text{GaAs}) = 0.45$, the effective mass of heavy holes in the lth sublayer is

$$m_l^{h^*} = \{0.45 + 0.062[(l-1)/j]\}m_0. \tag{44}$$

Now, $V_p^l(z)$ satisfies equation (39) still; so, if we substitute equations (39) and (44) into equations (28)–(33), the subbands and wavefunctions for heavy holes are determined by taking account of the variation in the effective mass of heavy holes as a function of z.

The wavefunctions of electrons and heavy holes obtained display obvious localised properties. Therefore, in addition to the potential of sawtooth shape, the redistribution of charge carriers will produce a self-consistent potential. We consider that the system is in the electric quantum limit, i.e. only the ground conduction and valence subbands are occupied. So the self-consistent potential is determined from the Poisson equation

$$\mathrm{d}V_H(z)/\mathrm{d}z^2 = -4\pi e^2 N_s/\varepsilon_s[|\Psi_e^0(z)|^2 - |\Psi_h^0(z)|^2] \tag{45}$$

where N_s is the area density of electrons or holes $\Psi_e^0(z)$ and $\Psi_h^0(z)$ are the ground wavefunctions of electrons and holes, respectively, and ε_s is the dielectric constant of $Ga_{1-x}Al_xAs$.

In our calculation, we neglect the small overlap between the wavefunctions of a primary cell and that of its nearest neighbours.

Table 1. Results for the subbands of electrons. E is the energy of the band edge, D is the width of the period and $\mathcal{K}$ is the Bloch wavevector. ATM is defined in the text, QMM is the quantum mechanics method and SCTBM is the self-consistent two-band method.

		E (meV)			
		$D = 140$ Å		$D = 210$ Å	
State	$\mathcal{K}$	ATM (SCTBM)	QMM	ATM (SCTBM)	QMM
Ground subband	0	61.8201	64.5040	51.1030	55.2795
Ground subband	π	70.1731	75,9940	52.1030	56.9035
First excitation subband	π	116.7621	178.9300	97.3571	102.0937
First excitation subband	0	150.7021	203.5730	106.6111	115.9878

Solving equation (45), we can obtain the self-consistent potential in a primary cell for electrons and holes:

$$V_{\mathrm{H}}^{\mathrm{e}}(z) = -\frac{4\pi e^2 N_{\mathrm{s}}}{\varepsilon_{\mathrm{s}}} \int_{z_n}^{z} \mathrm{d}z' \int_{z_n}^{z'} \mathrm{d}z \left[|\Psi_{\mathrm{e}}^{0}(z)|^2 - |\Psi_{\mathrm{h}}^{0}(z)|^2\right] \tag{46}$$

and

$$V_{\mathrm{H}}^{\mathrm{h}}(z) = -V_{\mathrm{H}}^{\mathrm{e}}(z). \tag{47}$$

Here, for convenience of calculation, we have moved the origin of the nth primary cell to the minimum point Z_n of the ground wavefunction of electrons that was obtained in the non-self-consistent calculation, as shown in figure 1(a).

The total potentials for electrons and holes are

$$V_{\mathrm{s}}^{\mathrm{sc}}(z) = V_{\mathrm{s}}(z) + V_{\mathrm{H}}^{\mathrm{e}}(z) \tag{48}$$

and

$$V_{\mathrm{p}}^{\mathrm{sc}}(z) = V_{\mathrm{p}}(z) + V_{\mathrm{H}}^{\mathrm{h}}(z). \tag{49}$$

Next we calculate the $V_{\mathrm{s}}^{\mathrm{sc}}(z)$ and $V_{\mathrm{p}}^{\mathrm{sc}}(z)$ in each sublayer and consider them as constants again within each sublayer. If we put them into equations (16) and (18) and repeat all the calculations above, we obtain the self-consistent results for subbands and wavefunctions.

The parameters taken for numerical calculations are $D = 210$ Å, $j = 200$, $\varepsilon_{\mathrm{s}} = 14$ and $N_{\mathrm{s}} = 0.5 \times 10^{11}\,\mathrm{cm}^{-2}$.

Because the effect of the redistribution of electrons and holes cancel each other, the self-consistent potential is small and so the modifications of subbands and wavefunctions in the self-consistent calculation is small; we stop the calculation after the first cycle of self-consistent calculations.

The results for the wavefunctions for both electrons and heavy holes are shown in figure 3. The corresponding results for subbands of electrons are listed in table 1 for comparison with the results in [4].

We can see from table 1 that not only are the energy values of the subbands of electrons in our results lower than those in [4], but also the widths of electron subbands are obviously smaller than those in [4]. For example, when $D = 210$ Å, the width of the

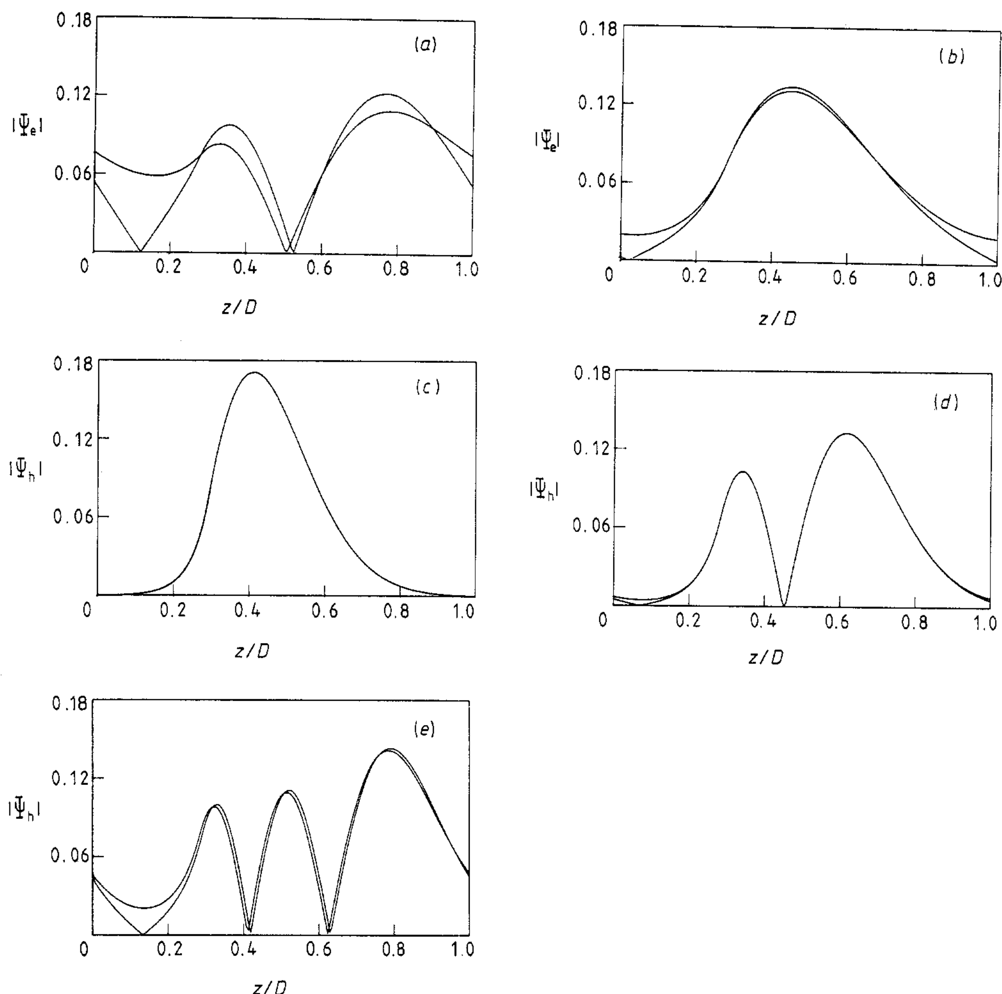

Figure 3. A plot of the moduli of wavefunctions of electrons ((*a*) first excitation subband; (*b*) ground subband) and heavy holes ((*c*) ground subband; (*d*) first excitation subband; (*e*) second excitation subband) as functions of the coordinate z inside a primary cell calculated by ATM. The parameters are $D = 210$ Å, $x = 0.2$, $j = 200$, $\varepsilon_s = 14$, $N_s = 0.5 \times 10^{11}$ cm^{-2}. In (*a*) the curve that has two nodes corresponds to $\mathcal{K} = 0$, $E = 106.6111$ meV and the other curve to $\mathcal{K} = \pi$, $E = 97.3571$ meV. In (*b*) the curve that has no node corresponds to the band edge with $\mathcal{K} = 0$, $E = 51.1030$ meV, and the other curve to $\mathcal{K} = \pi$, $E = 52.1030$ meV. In (*c*) the energies of the band edges are $E = 23.2777$ meV ($\mathcal{K} = 0$) and $E = 23.2781$ meV ($\mathcal{K} = \pi$), respectively. Because the band width is very small, the wavefunctions that correspond to the band edges are hard to distinguish from each other. In (*d*) the curve that has one node corresponds to the band edge with $\mathcal{K} = \pi$, $E = 44.0501$ meV, and the other curve to $\mathcal{K} = 0$, $E = 44.0682$ meV. In (*e*) the curve that has two nodes corresponds to the band edge with $\mathcal{K} = 0$, $E = 60.7700$ meV and the other curve to $\mathcal{K} = \pi$, $E = 61.0280$ meV.

ground subband and first excitation subband are 1.000 meV and 9.254 meV, respectively, in our results, but they are 1.624 meV and 13.8941 meV, respectively, in the results in [4]. To judge from the results of the more rigorous theory [6], our results are better than those in [4].

The ATM presented in this paper is universal and versatile and is suitable for dealing with both type-I and type-II semiconductor systems in which the band edges have a complex shape. The only limit is simply the limit for the envelope function approximation, i.e. the variation in the envelope function must not be too fast. This limit is equivalent to the fact that λ defined in equation (40) must not be too large. In our calculation we chose $j = 200$ to make $\lambda = 1$ meV Å^{-1}. Our results show that this gives enough accuracy for the discussion in this paper. Moreover, the wavefunctions obtained in the self-consistent calculation vary very slowly as a function of z.

Work on another calculation of type-II semiconductor multi-quantum-well systems [2] is under way, and we have started to investigate the elecronic states of the InAs quantum well buried a few tens of nanometres below a GaSb surface [7] in terms of ATM.

Midway through our calculation, we noticed the work in [8] which was the same idea as ours and gives a calculation of the bound states of a parabolic well.

Acknowledgment

This research is supported partly by the National Science Foundation of China.

References

[1] Guoyi Qin 1988 *J. Phys. C: Solid State Phys.* **21** 4989
[2] Bleuse J, Bastard G and Voisin P 1988 *Phys. Rev. Lett.* **60** 220
[3] Bastard G 1982 *Phys. Rev.* B **25** 7584
[4] Brum J A, Voisin P and Bastard G 1986 *Phys. Rev.* B **33** 1063
[5] Meynadier M H, Delalande C, Bastard G and Voos M 1985 *Phys. Rev.* B **31** 5539
[6] Jaros M, Wong K B and Gell M A 1985 *Phys. Rev.* B **31** 1205
[7] Altarelli M, Maan J C, Chang L L and Esaki L 1987 *Phys. Rev.* B **35** 9867
[8] Perez-Alvarez R, Rodriquez-Coppola H, Velasco V R and Garcia-Moliner F 1988 *J. Phys. C: Solid State Phys.* **21** 2197